ISSN 1674-1056
http://cpb.iphy.ac.cn
http://iopscience.iop.org/cpb
中国物理 B
Chinese Physics
中国物理 Chinese Physics B

Influence of fluorescence time characteristics on the spatial resolution of CW-stimulated emission depletion microscopy

Haiyun Qin(秦海芸), Wei Zhao(赵伟), Chen Zhang(张琛), Yong Liu(刘勇), Guiren Wang(王归仁), Kaige Wang(王凯歌)
Citation: Chin. Phys. B . 2018, 27(3): 037803. **doi:** 10.1088/1674-1056/27/3/037803

Journal homepage: http://cpb.iphy.ac.cn; http://iopscience.iop.org/cpb

What follows is a list of articles you may be interested in

Investigation of europium(Ⅲ)-doped ZnS for immunoassay

Chao-Fan Zhu(朱超凡), Xue Sha(沙雪), Xue-Ying Chu(楚学影), Jin-Hua Li(李金华), Ming-Ze Xu(徐铭泽), Fang-Jun Jin(金芳军), Zhi-Kun Xu(徐志堃)
Chin. Phys. B . 2018, 27(2): 027803. **doi:** 10.1088/1674-1056/27/2/027803

Substitution priority of Eu^{2+} in multi-cation compound $Sr_{0.8}Ca_{0.2}Al_2Si_2O_8$ and energy transfer

Zhi-Ping Yang(杨志平), Zhen-Ling Li(李振玲), Zhi-Jun Wang(王志军), Pan-Lai Li(李盼来), Miao-Miao Tian(田苗苗), Jin-Ge Cheng(程金阁), Chao Wang(王超)
Chin. Phys. B . 2018, 27(1): 017802. **doi:** 10.1088/1674-1056/27/1/017802

Electronic structure and photoluminescence property of a novel white emission phosphor $Na_3MgZr(PO_4)_3:Dy^{3+}$ for warm white light emitting diodes

Ge Zhu(朱革), Zhuo-Wei Li(李卓为), Chuang Wang(王闯), Fa-Guang Zhou(周发光), Yan Wen(温艳), Shuang-Yu Xin(辛双宇)
Chin. Phys. B . 2017, 26(9): 097801. **doi:** 10.1088/1674-1056/26/9/097801

Profile function properties & optical transition formulae

Qing-li Zhang(张庆礼), Guihua Sun(孙贵花), Jin-yun Gao(高进云), Dun-lu Sun(孙敦陆), Jian-qiao Luo(罗建乔), Wen-peng Liu(刘文鹏), De-ming Zhang(张德明), Chaoshu Shi(施朝淑), Shaotang Yin(殷绍唐)
Chin. Phys. B . 2017, 26(7): 077803. **doi:** 10.1088/1674-1056/26/7/077803

Full-profile fitting of emission spectrum to determine transition intensity parameters of Yb^{3+}: $GdTaO_4$

Qingli Zhang(张庆礼), Guihua Sun(孙贵花), Kaijie Ning(宁凯杰), Chaoshu Shi(施朝淑), Wenpeng Liu(刘文鹏), Dunlu Sun(孙敦陆), Shaotang Yin(殷绍唐)
Chin. Phys. B . 2016, 25(11): 117802. **doi:** 10.1088/1674-1056/25/11/117802

Influence of fluorescence time characteristics on the spatial resolution of CW-stimulated emission depletion microscopy*

Haiyun Qin(秦海芸)[1,†], Wei Zhao(赵伟)[1,†], Chen Zhang(张琛)[1], Yong Liu(刘勇)[2], Guiren Wang(王归仁)[3], and Kaige Wang(王凯歌)[1,‡]

[1] *Institute of Photonics and Photon-Technology, Northwest University, Xi'an* 710069, *China*
[2] *School of Electronics and Information Engineering, Shanghai University of Electric Power, Shanghai* 200090, *China*
[3] *Mechanical Engineering Department & Biomedical Engineering Program, University of South Carolina, Columbia, SC* 29208, *USA*

(Received 13 November 2017; revised manuscript received 13 December 2017; published online 11 February 2018)

As one of the most important realizations of stimulated emission depletion (STED) microscopy, the continuous-wave (CW) STED system, constructed by using CW lasers as the excitation and STED beams, has been investigated and developed for nearly a decade. However, a theoretical model of the suppression factors in CW STED has not been well established. In this investigation, the factors that affect the spatial resolution of a CW STED system are theoretically and numerically studied. The full-width-at-half-maximum (FWHM) of a CW STED with a doughnut-shaped STED beam is also reanalyzed. It is found that the suppression function is dominated by the ratio of the local STED and excitation beam intensities. In addition, the FWHM is highly sensitive to both the fluorescence rate (inverse of fluoresce lifetime) and the quenching rate, but insensitive to the rate of vibrational relaxation. For comparison, the suppression function in picosecond STED is only determined by the distribution of the STED beam intensity scaled with the saturation intensity. Our model is highly consistent with published experimental data for evaluating the spatial resolution. This investigation is important in guiding the development of new CW STED systems.

Keywords: stimulated emission depletion, continuous-wave laser, suppression function, numerical simulation

PACS: 78.45.+h, 78.55.–m **DOI:** 10.1088/1674-1056/27/3/037803

1. Introduction

Stimulated emission depletion (STED) microscopy is a novel super-resolution optical method that has been developed over the last two decades.[1,2] To achieve high spatial and temporal resolutions, various technical methods have been advanced.[3,4] In the beginning, the STED technique was realized by using picosecond pulsed lasers for both excitation and STED beams. By accurately synchronizing the excitation and depletion laser pulses, a highly depleted fluorescent spot with a significantly reduced size can be achieved. By using a doughnut-shaped STED beam, the spatial resolution can be enhanced from $\lambda/(2NA)$ (confocal microscopy) to $0.45\lambda/\left(NA\sqrt{1+I_{\mathrm{STED}}^{\mathrm{max}}/I_{\mathrm{sat}}}\right)$ (STED),[5] where λ and NA denote the wavelength of the excitation beam and the numerical aperture of the objective, respectively. $I_{\mathrm{STED}}^{\mathrm{max}}$ and I_{sat} are the maximum intensity of the STED beam and the saturation intensity of the fluorescence at which the probability of fluorescence emission is reduced by half, respectively. This theoretical model well describes the experimental studies of time-resolved fluorescent dynamics for dyes under exposure to picosecond pulses.

Meanwhile, a STED system based on continuous-wave (CW) lasers has also been developed.[6–9] Recently, the spatial resolution of CW-laser-based STED (CW STED) microscopes has been reported to typically be over 50 nm, which is less than that obtained for picosecond STED. However, CW STED is much easier to use than picosecond STED because it avoids the requirement of temporal synchronization of the excitation and STED beams, unlike picosecond STED. This is a great advantage for developing low-cost STED systems. Furthermore, many CW-laser-based techniques, such as the recently developed laser-induced fluorescence photobleaching anemometer, can be directly realized on the basis of a CW STED system.[6]

One of the primary obstacles in the development of a CW STED microscopy is the incomplete understanding of the suppression function. Currently, CW STED studies evaluate the suppression function and the corresponding spatial resolution based on theories advanced for picosecond STED, where the suppression function is normally expressed as $\eta(x) = \mathrm{e}^{-\ln 2 I_{\mathrm{sted}}/I_{\mathrm{sat}}}$. Here, I_{sted} is the intensity of the STED beam. However, the instant and fast fluorescent dynamic process in a

*Project supported by the National Natural Science Foundation of China (Grant Nos. 11672229 and 61378083), International Cooperation Foundation of the National Science and Technology Major Project of the Ministry of Science and Technology of China (Grant No. 2011DFA12220), Major Research Plan of the National Natural Science Foundation of China (Grant No. 91123030), Natural Science Foundation of Shaanxi Province of China (Grant Nos. 2010JS110 and 2013SZS03-Z01), Natural Science Basic Research Program of Shaanxi Province - Major Basic Research Project, China (Grant No. 2016ZDJC-15), Young Scientist Fund of the National Natural Science Foundation of China (Grant No. 11504294), and the Youth Talent Plan of the Natural Science Foundation of Shaanxi Province of China (Grant No. 2016JQ103).

†These authors contributed equally to this work.
‡Corresponding author. E-mail: wangkg@nwu.edu.cn

© 2018 Chinese Physical Society and IOP Publishing Ltd

picosecond STED system is different from that in a CW STED system, where the fluorescent dynamic process is statistically steady. Therefore, the aforementioned theoretical resolution prediction for picosecond STED may not be accurate for CW STED.

In this study, we reanalyze the fluorescent dynamics of the CW STED system and theoretically derive the suppression function. The full-width-at-half-maximum (FWHM) of the point-spreading function (PSF) for the effective fluorescent spot in CW STED with a Gaussian excitation beam and a doughnut-shaped STED beam is studied in detail. The theoretical results are validated by published experimental data from other studies. Finally, the influence of the control time parameters, such as the rates of quenching, fluorescence, and vibrational relaxation, is investigated.

2. Theory of a CW STED system

The general excitation and emission processes of a fluorophore are plotted in Fig. 1(a). As suggested by Hell and Wichmann,[2] the corresponding probability (n_i) of electrons on each level L_i can be expressed as

$$\begin{cases} \dfrac{\mathrm{d}n_0}{\mathrm{d}t} = h_{\mathrm{exc}}s_{\mathrm{exc}}(n_1 - n_0) + k_{\mathrm{vib}}n_3, \\ \dfrac{\mathrm{d}n_1}{\mathrm{d}t} = h_{\mathrm{exc}}s_{\mathrm{exc}}(n_0 - n_1) - k_{\mathrm{vib}}n_1, \\ \dfrac{\mathrm{d}n_2}{\mathrm{d}t} = k_{\mathrm{vib}}n_1 + h_{\mathrm{sted}}s_{\mathrm{sted}}(n_3 - n_2) - (k_{\mathrm{fl}} + k_{\mathrm{Q}})n_2, \\ \dfrac{\mathrm{d}n_3}{\mathrm{d}t} = -k_{\mathrm{vib}}n_3 - h_{\mathrm{sted}}s_{\mathrm{sted}}(n_3 - n_2) + (k_{\mathrm{fl}} + k_{\mathrm{Q}})n_2, \end{cases} \tag{1}$$

where $h_{\mathrm{exc}}(x) = I_{\mathrm{exc}}(x)/\hbar\nu_{\mathrm{exc}}$ and $h_{\mathrm{sted}}(x) = I_{\mathrm{sted}}(x)/\hbar\nu_{\mathrm{sted}}$ are the normalized intensities of excitation and STED beams in which ν_{exc} and ν_{sted} are the frequencies of excitation and depletion photons, respectively. $\hbar$ is the reduced Planck constant. s_{exc} and s_{sted} are the cross sections for the absorptions. k_{vib}, k_{fl}, and k_{Q} are the average rates of the vibrational relaxation, fluorescence, and quenching, respectively. In the CW STED system, the excitation and STED beam power intensities, h_{exc} and h_{sted}, are temporally constant. The fluorescence process is steady, and the probability n_i in each state L_i is also statistically constant in time. This can be seen by averaging Eq. (1) temporally as

$$\begin{cases} h_{\mathrm{exc}}s_{\mathrm{exc}}(\overline{n_1} - \overline{n_0}) + k_{\mathrm{vib}}\overline{n_3} = 0, \\ h_{\mathrm{exc}}s_{\mathrm{exc}}(\overline{n_0} - \overline{n_1}) - k_{\mathrm{vib}}\overline{n_1} = 0, \\ k_{\mathrm{vib}}\overline{n_1} + h_{\mathrm{sted}}s_{\mathrm{sted}}(\overline{n_3} - \overline{n_2}) - (k_{\mathrm{fl}} + k_{\mathrm{Q}})\overline{n_2} = 0, \\ -k_{\mathrm{vib}}\overline{n_3} - h_{\mathrm{sted}}s_{\mathrm{sted}}(\overline{n_3} - \overline{n_2}) + (k_{\mathrm{fl}} + k_{\mathrm{Q}})\overline{n_2} = 0, \end{cases} \tag{2}$$

where the bar indicates temporal averaging. $\overline{n_i}$ represents the mean probability for each excitation level. Let $\widetilde{k_{\mathrm{Q}}} = k_{\mathrm{Q}}/h_{\mathrm{exc}}s_{\mathrm{exc}}$, $\widetilde{k_{\mathrm{fl}}} = k_{\mathrm{fl}}/h_{\mathrm{exc}}s_{\mathrm{exc}}$, $\widetilde{k_{\mathrm{vib}}} = k_{\mathrm{vib}}/h_{\mathrm{exc}}s_{\mathrm{exc}}$ and

$$\gamma = h_{\mathrm{sted}}s_{\mathrm{sted}}/h_{\mathrm{exc}}s_{\mathrm{exc}}, \tag{3}$$

then the solutions of Eq. (2) can be described as

$$\begin{bmatrix} n_0 \\ n_1 \\ n_2 \\ n_3 \end{bmatrix} = \frac{1}{\left(\widetilde{k_{\mathrm{Q}}} + \widetilde{k_{\mathrm{fl}}}\right)\left(\widetilde{k_{\mathrm{vib}}} + 3\right) + \widetilde{k_{\mathrm{vib}}} + \gamma\left(\widetilde{k_{\mathrm{vib}}} + 4\right)} \times \begin{bmatrix} \left(\widetilde{k_{\mathrm{vib}}} + 1\right)\left(\widetilde{k_{\mathrm{Q}}} + \widetilde{k_{\mathrm{fl}}} + \gamma\right) \\ \widetilde{k_{\mathrm{Q}}} + \widetilde{k_{\mathrm{fl}}} + \gamma \\ \widetilde{k_{\mathrm{vib}}} + \gamma \\ \widetilde{k_{\mathrm{Q}}} + \widetilde{k_{\mathrm{fl}}} + \gamma \end{bmatrix}. \tag{4}$$

Generally, the effective PSF for the STED microscopy can be described by the product of the PSF for the fluorescence on focus ($I_{\mathrm{exc}}(x)$) and a suppression function $\eta(x)$ as $I_{\mathrm{eff}}(x) = I_{\mathrm{exc}}(x)\,\eta(x)$.[10] Since $\eta(x) = n_2$,[2] the effective PSF of STED microscopy becomes

$$h_{\mathrm{eff}}(x) = h_{\mathrm{exc}}(x)\,n_2, \tag{5}$$

or equivalently, $I_{\mathrm{eff}}(x) = I_{\mathrm{exc}}n_2$. In a typical CW STED system, $s_{\mathrm{exc}} \approx s_{\mathrm{sted}} = 10^{-16}$ cm^2, and k_{vib}, k_{fl}, and k_{Q} are determined by the fluorescent dyes. I_{exc}, I_{sted}, and the corresponding γ can be calculated by numerical methods.

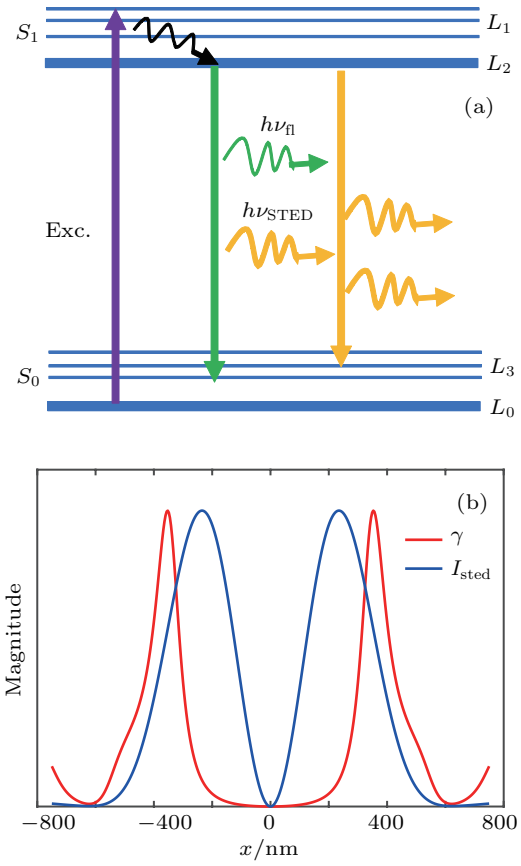


Fig. 1. (color online) (a) Schematic of the excitation, emission, and depletion processes of a fluorophore. (b) Schematic profiles of I_{sted} and γ for the lateral direction in the focus area of experimental case 2. Here, the wavelengths of the excitation and STED beams are 635 nm and 750 nm, respectively. To obtain these two profiles, both I_{exc} and I_{sted} distributions on the focal plane are numerically computed by Debye integral method first, with the experimental conditions of case 2. Then, γ is calculated on the basis of Eq. (7). The profiles have been normalized for comparison.

It can be schematically seen from Fig. 1(b) that for picosecond STED, the suppression function $\eta(x) = e^{-\ln(2) I_{sted}(x)/I_{sat}}$ is determined by the local intensity of the STED beam, i.e., $I_{sted}(x)$, while in CW STED, the suppression function is dominated by γ, which is the ratio of the STED and excitation intensities. The peaks of γ are located farther away from the center with narrower lobes. The peaks of $I_{sted}(x)$ are relatively closer to the center and have wider lobes. The different control parameters and their distribution may lead to different suppression results. Intuitively, picosecond STED should show better suppression for the tails of Gaussian excitation beams compared to CW STED and result in a smaller FWHM for $I_{eff}(x)$.

The FWHM of CW STED systems with a Gaussian excitation beam and a doughnut-shaped STED beam are theoretically studied below and compared with the FWHM of picosecond STED systems. Here, to simplify the analysis, we assume that the depletion due to the excitation beams has a high power ratio (e.g., > 1000).

In general, the PSF of the excitation and STED beams can be described as

$$h_{exc}(x) = H_{e0} \exp\left[-4\ln 2 \frac{x^2}{d_{exc}^2}\right], \tag{6a}$$

$$h_{sted}(x) = eH_{s0} \frac{4x^2}{d_{sted}^2} \exp\left[-4\frac{x^2}{d_{sted}^2}\right], \tag{6b}$$

where H_{e0} and H_{s0} are the peak values for $h_{exc}(x)$ and $h_{sted}(x)/e$, respectively. d_{exc} is the diameter of the Gaussian beam and d_{sted} is the diameter of the doughnut-like spot at peak. It should be noted that due to the far-red tail of the emission spectrum of the STED beam, s_{exc} is normally larger than s_{sted}. To simplify the model for theoretical analysis, the approximation of equal absorption cross-sections, i.e., $s_{sted} \approx s_{exc} = s$ is applied. Then, we have

$$\gamma = \frac{eH_{s0}}{H_{e0}} \frac{4x^2}{d_{sted}^2} \exp\left[-4x^2\left(\frac{1}{d_{sted}^2} - \frac{\ln 2}{d_{exc}^2}\right)\right]. \tag{7}$$

Normally, $\widetilde{k_{vib}} \gg \widetilde{k_Q} \sim \widetilde{k_{fl}} > 1$. By substituting Eq. (7) into Eq. (4), we obtain

$$\begin{aligned} n_2 &= \frac{\widetilde{k_{vib}} + \gamma}{\left(\widetilde{k_Q} + \widetilde{k_{fl}}\right)\left(\widetilde{k_{vib}} + 3\right) + \widetilde{k_{vib}} + \gamma\left(\widetilde{k_{vib}} + 4\right)} \\ &\approx \frac{\widetilde{k_{vib}} + \gamma}{\left(\widetilde{k_Q} + \widetilde{k_{fl}}\right)\widetilde{k_{vib}} + \widetilde{k_{vib}} + \gamma\widetilde{k_{vib}}} = \frac{1 + \dfrac{\gamma}{\widetilde{k_{vib}}}}{\widetilde{k_Q} + \widetilde{k_{fl}} + 1 + \gamma}, \end{aligned} \tag{8}$$

γ normally covers a large range of magnitudes. When I_{sted} is not sufficiently large, we have approximately $\gamma/\widetilde{k_{vib}} = h_{sted}(x) s_{sted}/k_{vib} \ll 1$. Then, equation (8) becomes

$$\begin{aligned} n_2 &\approx \frac{1}{\widetilde{k_Q} + \widetilde{k_{fl}} + 1 + \gamma} \\ &= \frac{\exp\left[-4\ln 2 \dfrac{x^2}{d_{exc}^2}\right]}{\dfrac{k_Q + k_{fl}}{H_{e0} s} + \exp\left[-4\ln 2 \dfrac{x^2}{d_{exc}^2}\right] + \dfrac{eH_{s0}}{H_{e0}} \dfrac{4x^2}{d_{sted}^2} \exp\left[-4\dfrac{x^2}{d_{sted}^2}\right]}. \end{aligned} \tag{9}$$

Since the FWHM of STED must be smaller than d_{exc} and d_{sted} in the range $|x| < d_{exc} < d_{sted}$, using the Taylor expansion, we have

$$\exp\left[-4\ln 2 \frac{x^2}{d_{exc}^2}\right] = \sum_{n=0}^{\infty} \frac{1}{n!} \left(-\frac{\ln 2}{d_{exc}^2}\right)^n (2x)^{2n}, \tag{10a}$$

$$\frac{4x^2}{d_{sted}^2} \exp\left[-4\frac{x^2}{d_{sted}^2}\right] = \sum_{n=1}^{\infty} \frac{(-1)^{n-1}}{(n-1)!} \left(\frac{1}{d_{exc}^2}\right)^n (2x)^{2n}. \tag{10b}$$

Thus, from Eq. (9), it can be seen that

$$n_2 = \frac{\exp\left[-4\ln 2 \dfrac{x^2}{d_{exc}^2}\right]}{\dfrac{k_Q + k_{fl}}{H_{e0} s} + 1 + \sum\limits_{n=1}^{\infty} \dfrac{(-1)^n (2x)^{2n}}{n!} \left[\left(\dfrac{\ln 2}{d_{exc}^2}\right)^n - \dfrac{eH_{s0}}{H_{e0}} n \left(\dfrac{1}{d_{sted}^2}\right)^n\right]}. \tag{11}$$

Since $|x| < d_{exc} < d_{sted}$, the denominator in Eq. (11) can be approximated by

$$\begin{aligned} &\frac{k_Q + k_{fl}}{H_{e0} s} + 1 + \sum_{n=1}^{\infty} \frac{(-1)^n (2x)^{2n}}{n!} \\ &\times \left[\left(\frac{\ln 2}{d_{exc}^2}\right)^n - \frac{eH_{s0}}{H_{e0}} n \left(\frac{1}{d_{sted}^2}\right)^n\right] \\ &\approx \frac{k_Q + k_{fl}}{H_{e0} s} + B \sin^2(\pi x P) = A\left[1 - M \frac{1 + \cos(2\pi x P)}{2}\right], \end{aligned} \tag{12}$$

where

$$P = \sqrt{\frac{(C - \ln 2)\ln 2 + BC^2}{BC - \ln 2}} / d_{exc},$$

$$A = \frac{k_Q + k_{fl}}{H_{e0} s} + B, \quad B = H_{s0}/H_{e0}, \quad C = d_{exc}^2/d_{sted}^2,$$

and $M = B/A$. This approximation has also been validated by numerical methods in the range $|x| < d_{exc} < d_{sted}$, as shown in Fig. 2. Then, n_2 from Eq. (11) can be approximated to

$$n_2 \approx \frac{\exp\left[-4\ln 2 \dfrac{x^2}{d_{exc}^2}\right]}{A\left[1 - M \dfrac{1 + \cos(2\pi x P)}{2}\right]}. \tag{13}$$

Substituting Eqs. (6a) and (13) into Eq. (5), one has

$$h_{\rm eff}(x) = A^{-1}H_{\rm e0}\exp\left[-8\ln 2\frac{x^2}{d_{\rm exc}^2}\right] \times\left[1-M\frac{1+\cos(2\pi xP)}{2}\right]^{-1}. \quad (14)$$

When $x=0$, $h_{\rm eff}(x)=H_{\rm e0}/A(1-M)$. Therefore, the FWHM can be determined at x where $h_{\rm eff}(x)=H_{\rm e0}/2A(1-M)$. By taking the logarithm of $h_{\rm eff}(x)$, we have

$$\ln\left(H_{\rm e0}\exp\left[-8\ln 2\frac{x^2}{d_{\rm exc}^2}\right)-\ln\left\{A\left[1-M\frac{1+\cos(2\pi xP)}{2}\right]\right\} = \ln\left[\frac{H_{\rm e0}}{2A(1-M)}\right]. \quad (15)$$

Since $[1+\cos(2\pi xP)]/2\leq 1$ and

$$M=1/\left(\frac{k_{\rm Q}+k_{\rm fl}}{H_{\rm s0}s}+1\right)<1,$$

the second term on the left-hand side of Eq. (15) can be simplified by a Taylor expansion to the order of $O(x^2)$. This leads to

$$\ln\left\{A\left[1-M\frac{1+\cos(2\pi xP)}{2}\right]\right\} \approx \ln A+\ln(1-M)+x^2\frac{\pi^2P^2M}{1-M}+O(x^4). \quad (16)$$

Then, equation (15) becomes

$$\ln H_{\rm e0}-8\ln 2\frac{x^2}{d_{\rm exc}^2}-\ln A(1-M)-\frac{\pi^2P^2M}{1-M}x^2 = \ln\left[\frac{H_{\rm e0}}{2A(1-M)}\right]. \quad (17)$$

Finally, the FWHM represented by $\Delta x_{\rm a}$ can be described as

$$\Delta x_{\rm a}=\frac{2\sqrt{\ln 2}}{\sqrt{\frac{8\ln 2}{d_{\rm exc}^2}+\frac{\pi^2P^2M}{1-M}}}=\frac{d_{\rm exc}}{N}, \quad (18)$$

where

$$N=\sqrt{2+\frac{\pi^2P^2Md_{\rm exc}^2}{4(1-M)\ln 2}}$$

is the factor of resolution improvement of the STED system compared to the confocal system. In the case of a high power ratio (>1000) of depletion to excitation beams, normally, $B\gg 1$ and $(k_{\rm Q}+k_{\rm fl})/H_{\rm e0}s\ll B$. Therefore, $A\to B$, $M\to 1$, and

$$N\approx\sqrt{2+\frac{\pi^2BCn_2(x=0)}{4\ln 2}}\sim\sqrt{BCn_2(x=0)}.$$

Here, $n_2(x=0)=((k_{\rm Q}+k_{\rm fl})/H_{\rm e0}s)^{-1}$ is the maximum population of electrons in L_2. This is proportional to the maximum fluorescent intensity.

Compared to the picosecond STED system whose resolution relies on the maximum and saturation intensities of the STED beam only, the spatial resolution of the CW STED is more complicated and is determined by γ, $k_{\rm Q}$, and $k_{\rm fl}$.

The FWHM of the CW STED beam at a large B is inversely proportional to $\sqrt{B}$. This is comparable to that for the picosecond STED beam, which implies that the CW STED beam has a potency equivalent to a picosecond STED beam for realizing a small FWHM. However, as shown in Fig. 3, the suppression function of the CW STED system is slightly different from that in the picosecond STED system. Around $x=0$, n_2 for the former is slightly narrower than $\eta(x)$ for the latter. This implies that from a simple comparison of the suppression functions for CW and picosecond STED systems under the same conditions of case 2, one can also realize a sharp peak for $I_{\rm eff}(x)$ in the CW STED system. Moreover, n_2 also exhibits a slower decreasing rate along x relative to $\eta(x)$. Therefore, the CW STED system with a doughnut-shaped STED beam should show a weaker suppression effect for the tails of Gaussian- type excitation beams. Consequently, the CW STED system should show relatively poorer suppression effect, spatial resolution, and signal-to-noise ratio compared to those of the picosecond STED system.

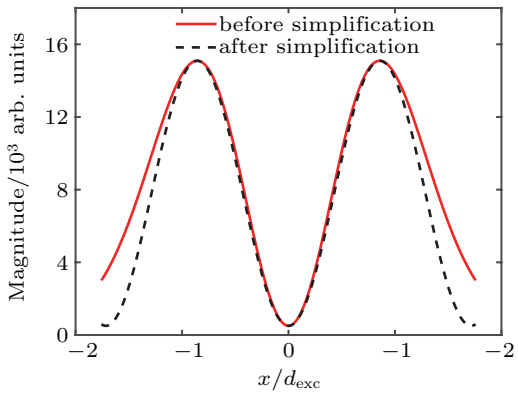


Fig. 2. (color online) Evaluation of the simplification of Eq. (11) to Eq. (13). It can be seen that in the range $|x/d_{\rm exc}|<1$, a good agreement is achieved before and after the simplification.

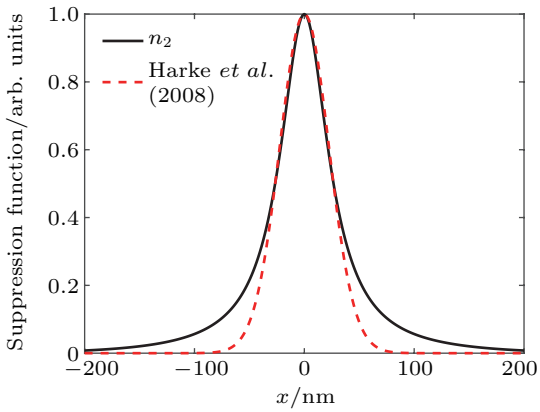


Fig. 3. (color online) Comparison of the suppression functions in the CW STED model (n_2) and in the picosecond STED system (i.e., $\eta(x)\cong\exp[-\ln(2)I_{\rm sted}(x)/I_{\rm sat}]$).[10] The simulations of the two suppression functions are both based on the conditions of case 2 in Table 1.

In addition, for the picosecond STED system, one can increase the resolution by increasing the intensity of the STED beam or decreasing the saturation intensity, which is an experimental parameter of the fluorescent dyes. However, the method for effectively decreasing the saturation intensity is not yet fully understood. For the CW STED system, we find

$$N\sim\sqrt{n_2(x=0)}=\sqrt{\left(\frac{k_{\mathrm{Q}}+k_{\mathrm{fl}}}{H_{\mathrm{e0}}s}\right)^{-1}},$$

which straight-forwardly elucidates the relationship between the fluorescent dye and spatial resolution and implies that one can enhance the spatial resolution by inhibiting k_{Q} and k_{fl}. This has the potential to be a significant advance for developing new CW STED systems.

3. Validation of the theoretical model

3.1. Numerical simulation of the excitation and depletion beams of CW STED

To give a straightforward explanation for the depletion process of CW STED and the resulting $I_{\mathrm{eff}}(x)$, a numerical method implemented by Matlab based on the vector diffraction theory and the generalized Debye integral[11] is adopted. The electric-field vector can be described as

$$\begin{aligned}&\boldsymbol{E}(r_p,\varphi_p,z_p)\\&=\iint\sqrt{\cos\theta}\cdot\sin\theta\cdot E(\theta,\varphi)\cdot\boldsymbol{V}(\theta,\varphi)\boldsymbol{P}(x,y,z)\cdot\mathrm{e}^{\mathrm{i}\Delta\alpha(\theta,\varphi)}\\&\times\mathrm{e}^{\mathrm{i}kn(z_p\cdot\cos\theta+r_p\cdot\sin\theta\cdot\cos(\varphi-\varphi_p)}\,\mathrm{d}\varphi\,\mathrm{d}\theta,\end{aligned}\tag{19}$$

where r_p, φ_p, and z_p are the radial, azimuthal, and axial components in the cylindrical coordinates, respectively, as plotted in Fig. 4(a). $\boldsymbol{E}(r_p,\varphi_p,z_p)$ is the electric-field vector at the point (r_p,φ_p,z_p). $\sqrt{\cos\theta}$ represents the apodization factor resulting from energy conservation and geometric considerations.[12] NA is the numerical aperture of the objective. $n=1.52$ is the medium refractive index. θ denotes the angle between the ray direction and optical axis, where $0\le\theta\le\theta_{\max}$, with $\theta_{\max}=\sin^{-1}(NA/n)$. $E(\theta,\varphi)$ and $\boldsymbol{P}(x,y,z)$ are the amplitude function and polarization vector of the incident beam, respectively. $\mathrm{e}^{\mathrm{i}\Delta\alpha(\theta,\varphi)}$ is the phase delay function. $\boldsymbol{V}(\theta,\varphi)$ is the conversion matrix of the polarization from the object field to the image field, which is given as

$$\boldsymbol{V}(\theta,\varphi)=\begin{bmatrix}1+(\cos\theta-1)\cos^2\varphi & (\cos\theta-1)\cos\varphi\sin\varphi & -\sin\theta\cos\varphi\\(\cos\theta-1)\cos\varphi\sin\varphi & 1+(\cos\theta-1)\sin^2\varphi & -\sin\theta\sin\varphi\\\sin\theta\cos\varphi & \sin\theta\sin\varphi & \cos\theta\end{bmatrix}.\tag{20}$$

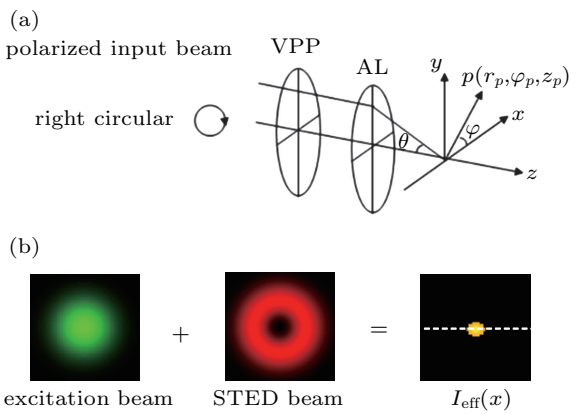


Fig. 4. (color online) (a) Coordinate system of the simulation. r_p, φ_p, and z_p are the radial, azimuthal, and axial components in the cylindrical coordinates, respectively. θ denotes the angle between the incident light and the optical axis. AL represents an achromatic lens. z is the axial direction of the incident beam. x and y are the axes perpendicular to the optical axis. (b) Illustration of the excitation beam (green), STED beam (red), and the resulting $I_{\mathrm{eff}}(x)$ (yellow). Here, experimental case 2 is plotted for reference.

The laser beam intensity evaluated by the magnitude of $\boldsymbol{E}$ can be expressed as $I=|\boldsymbol{E}_x^2|+|\boldsymbol{E}_y^2|+|\boldsymbol{E}_z^2|$. Therefore, the corresponding distribution of I can be computed based on the optical system. In this investigation, several reported experimental studies[9,13,14] are revisited numerically. All of these reports have used a right-handed circularly polarized (RCP) beam, with $\boldsymbol{P}(x,y,z)=\frac{1}{\sqrt{2}}(1,\mathrm{i},0)$, and a vortex phase plate (VPP) to generate a doughnut-shaped depletion beam. The phase delay function can be described by $\mathrm{e}^{\mathrm{i}\varphi}$ $(0\le\varphi\le\pi)$.

In this simulation, both $I_{\mathrm{exc}}(x)$ and $I_{\mathrm{sted}}(x)$ are first numerically computed. Then, γ is computed accordingly. Depending on γ, k_{Q}, k_{fl}, and k_{vib}, the suppression function of CW STED is further investigated based on n_2 in Eq. (4). Subsequently, $I_{\mathrm{eff}}(x)$ is obtained from Eq. (5) and the FWHM for $I_{\mathrm{eff}}(x)$ is evaluated accordingly. In addition, Δx_{a} can also be calculated from Eq. (18). Finally, the experimental resolution and the numerical and theoretical FWHM are compared and summarized in Table 1.

3.2. Results

The key parameters for the four revisited CW STED systems including the wavelength and power of the excitation (λ_{exc}) and STED (λ_{sted}) beams and fluorescent dyes with their relevant time constants are all summarized in Table 1. These STED systems all use Gaussian excitation beams and doughnut-shaped STED beams, as illustrated in Fig. 4(b). For instance, in the setup of Willig *et al.* (2007)[9] (case 2), the numerical simulations of the excitation and depletion beams at the focus are plotted in Fig. 4(b). Based on the numerically

simulated depletion beam, the suppression function $\eta(x)$ can be directly obtained, with its profile plotted in Fig. 3. The resulting $I_{\rm eff}(x)$ based on the depletion theory of CW STED introduced in this manuscript is illustrated in Fig. 4(b). The corresponding FWHM along the dashed line, e.g., $\Delta x_{\rm n}$, is thus calculated. It can be seen that the spatial resolution ($\Delta x_{\rm exp}$) measured in the experiment is 52 nm. The corresponding $\Delta x_{\rm n}$, which is equivalent to the spatial resolution of the STED system, is calculated to be 52 nm by numerical simulation. In comparison, by using Eq. (18), we obtain $\Delta x_{\rm a} = 45$ nm. Both $\Delta x_{\rm n}$ determined by numerical simulation and $\Delta x_{\rm a}$ calculated by Eq. (18) are sufficiently close to the experimental results. In all four cases, the theoretical model matches well with the experimental results, as shown in Table 1 and plotted in Fig. 5(a). The relative error evaluated by $\varepsilon = \left(\Delta x_{\rm exp} - \Delta x_{\rm n}\right)/\Delta x_{\rm n} \times 100\%$ indicates that the difference between experiment and theory is within 10% in all four cases. Therefore, the four independent experimental datasets well support our theoretical model. The error could be due to several reasons, such as, inaccurate values for the power of the excitation and STED beams given in the references. Normally, laser powers are measured before the pupil of the objective, which can lead to an overestimation for the incident laser power. Additionally, the estimation of the spatial resolution of STED in the experiments can also be inaccurate. The FWHM of $I_{\rm eff}(x)$ is sensitive to $k_{\rm Q}$ and $k_{\rm fl}$, which can be influenced by many factors, such as temperature, dye concentration, laser power density, and so on.[18] This will also lead to errors between theory and experiments. In addition, the inevitable photobleaching can also result in error.

Table 1. Comparison between the experimental and computational results for the resolution (or FWHM) of a STED system based on four experimental cases.

Case	Reference	Original experimental data				Dye	Resolution $\Delta x_{\rm exp}$/nm	$k_{\rm vib}$/s^{-1}	$k_{\rm fl}$/s^{-1}	$k_{\rm Q}$/s^{-1}	$\Delta x_{\rm n}$ /nm	$\Delta x_{\rm a}$/nm
		Excitation beam		STED beam								
		$\lambda_{\rm exc}$/nm	Power/mW	$\lambda_{\rm STED}$/nm	Power/mW							
1	Hein *et al.* (2008)[13]	488	0.003	592	112	YFP citrine	60	10^{12}	3×10^{8} [15]	10^{8}	65	58
2	Willig *et al.* (2007)[9]	635	0.0067	750	423	Atto 647N	52	10^{12}	3×10^{8} [a]	10^{9}	52	45
3	Willig *et al.* (2007)[9]	532	0.025	647	114	Atto 565	61	10^{12}	3×10^{8} [a]	5×10^{8}	61	53
4	Hotta *et al.* (2010)[14]	633	0.0025	780	58	pTDI	78	10^{12}	4×10^{8} [16]	10^{8}	85	76

[a] Official data collected from Sigma-Aldrich.

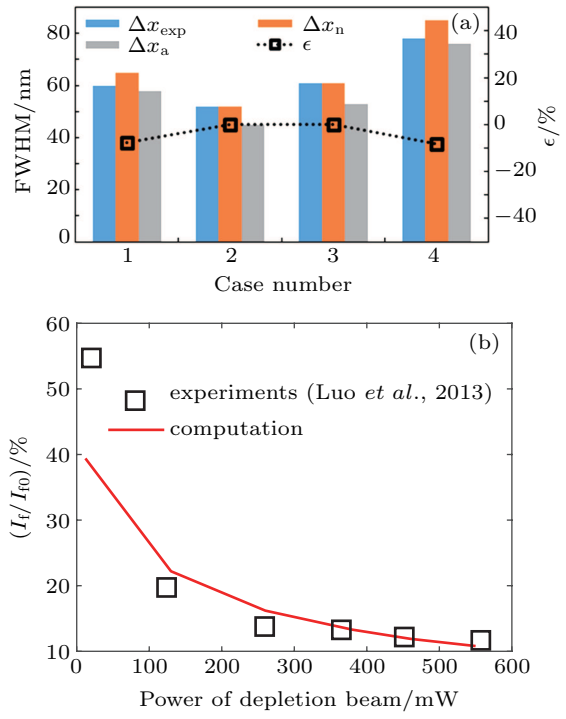


Fig. 5. (color online) (a) Comparison of the experimental and numerical results summarized in Table 1. (b) Comparison of the numerical results with the experimental results from Luo *et al.*,[17] where 405 nm (50 μW) and 532 nm lasers were used as excitation and STED beams, respectively. The fluorescent dye used is Atto 390. $I_{\rm f0}$ and $I_{\rm f}$ represent the fluorescent signals before and after depletion, respectively. Here, $k_{\rm fl} = 2\times10^{8}$ s^{-1} (official data from ATTO-TEC), $k_{\rm Q} = 4\times10^{9}$ s^{-1} (nonlinearly fitted by the experimental data), and $k_{\rm vib} = 10^{12}$ s^{-1}.

We also compare our theory with the investigation of Luo *et al.*,[17] who studied the remnant fluorescent intensity ($I_{\rm f}/I_{\rm f0}$) under various powers of the STED beam, as plotted in Fig. 5(b). It is interesting to note that except for the STED beam with low power (12 mW), all other experimental points are well matched by the theoretical predictions. Currently, for a sufficiently high STED beam power, our theory can be used to accurately predict the depletion process of a STED system. The discrepancy observed between theory and experiment at low powers is still not yet clear. One of the possible reasons for this difference is that the statistically steady state predicted in Eq. (2) does not apply in the low γ region. When the power of the STED beam is sufficiently high, the low γ region can be inhibited and its influence on the model is significantly limited. However, if the power of the STED beam is low, a large region with a low γ can exist. Consequently, the steady-state based model becomes invalid. This can result in a large discrepancy between the model and experiment.

4. Discussion

When the optical parameters, such as wavelength, power, and beam shape, are fixed, the spatial resolution (or FWHM) of the CW STED system is determined by the time constants of the fluorescent dye, i.e., $k_{\rm Q}$, $k_{\rm fl}$, and $k_{\rm vib}$.

We have also analyzed the influence of the time constants on the FWHM of $I_{\rm eff}(x)$, as shown in Fig. 6. It can be seen from Fig. 6(a) that for the $k_{\rm fl}$ range considered, $\Delta x_{\rm n}$ increases

rapidly with $k_{\rm fl}$ increasing from 46 nm to 117 nm. To reduce $\Delta x_{\rm n}$, one can use fluorescent dyes with a smaller $k_{\rm fl}$. This theoretical result is supported by the experimental observations of Neupane *et al.*,[7] who found that the FWHM of a CW STED system qualitatively increased with increasing $k_{\rm fl}$ in the range of 10^8 s^{-1} to 2×10^9 s^{-1}.

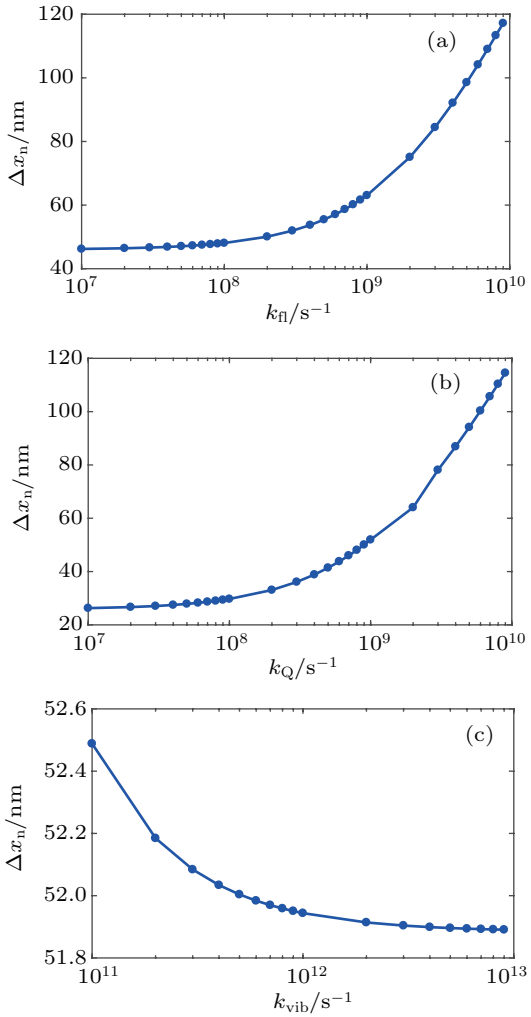


Fig. 6. (color online) Influence of the time constants on the FWHM of $I_{\rm eff}(x)$, i.e., $\Delta x_{\rm n}$. The computation is based on case 2. (a) Influence of the rate of fluorescence, where $k_{\rm Q} = 10^9$ s^{-1} and $k_{\rm vib} = 10^{12}$ s^{-1}. (b) Influence of the rate of quenching, where $k_{\rm fl} = 3\times10^8$ s^{-1} and $k_{\rm vib} = 10^{12}$ s^{-1}. (c) Influence of the rate of relaxation, where $k_{\rm fl} = 3\times10^8$ s^{-1} and $k_{\rm Q} = 10^9$ s^{-1}.

Similar results are also shown in Fig. 6(b), where the relation between $k_{\rm Q}$ and $\Delta x_{\rm n}$ is plotted. For $k_{\rm Q}$ in the range of 10^7 s^{-1} to 10^{10} s^{-1}, $\Delta x_{\rm n}$ increases from 26 nm to 114 nm. In the most commonly used range, i.e., 10^8 s^{-1} to 10^9 s^{-1}, $\Delta x_{\rm n}$ varies from 30 nm to 52 nm. A variation in $\Delta x_{\rm n}$ of more than 50% can be found. The results above show that both the fluorescent lifetime and quenching time of the dye can significantly influence the FWHM of a CW STED system. Therefore, these system parameters should be accurately determined by independent measurements. However, recent studies have ignored the influence of $k_{\rm Q}$ when building CW STED systems. Furthermore, due to the complicated mechanism of quenching, it is difficult for researchers to measure the quenching rate of fluorophores.[18] We consider this to be the major obstacle in the application of our model.

The influence of vibrational relaxation has also been evaluated via $k_{\rm vib}$. For $k_{\rm vib}$ in the range of 10^{11} s^{-1} to 10^{13} s^{-1}, the variation in $\Delta x_{\rm n}$ for $I_{\rm eff}(x)$ is less than 0.6 nm. Compared to $k_{\rm Q}$ and $k_{\rm fl}$, $k_{\rm vib}$ has negligible effect on the FWHM of CW STED, as plotted in Fig. 6(c).

In picosecond STED systems, where the fluorescence process in fluorophores is related to the time and pulse-width, the dependency of the spatial resolution (or FWHM of $I_{\rm eff}(x)$) on $k_{\rm Q}$ and $k_{\rm fl}$ is implicit, as discussed by Westphal and Hell.[19] However, $\Delta x_{\rm n}$ is observed to be strongly dependent on $k_{\rm Q}$ and $k_{\rm fl}$ in the CW STED system for which the fluorescent process of the fluorophores is statistically steady. This is very interesting. From Eq. (1), when $k_{\rm Q}$ and $k_{\rm fl}$ are sufficiently small (equivalent to a large fluorescent lifetime and quenching time), the population of the electrons in L_2 is primarily dominated by n_1 (which is determined by the intensity of the excitation beam) and the intensity of the STED beam. Hence, depletion at locations with high γ can be more easily achieved. Nevertheless, when $k_{\rm Q}$ and $k_{\rm fl}$ are large, the decay process for n_2 is proportional to the term $\mathrm{e}^{-(h_{\rm sted}s_{\rm sted}+k_{\rm fl}+k_{\rm Q})t}$. The population at L_2 decreases much faster through the spontaneous fluorescence process instead of the depletion process. Consequently, depletion is weakened, which results in a larger FWHM for $I_{\rm eff}(x)$. It should be noted that the quenching mechanism and its time constant rely on many factors, such as the concentration of the fluorescent reagent, temperature, and additives.[20] As the concentration of the dye is increased, the molecular interaction is strengthened. This leads to fluorescent extinction through the process of fluorophore composition or non-radiative transition.[20] This may explain why it is normally difficult to reach high depletion efficiency at high concentrations of fluorescent dye.

5. Conclusion

In this manuscript, the depletion process for a CW STED system is reanalyzed. The results indicate that from the viewpoint of the suppression function, the depletion process in a CW STED system is not exactly the same as that in a picosecond STED system. The picosecond STED system is more dependent on the STED beam, while the CW STED system is more significantly affected by the intensity ratio of the STED to excitation beams, i.e., the relative intensity between the two beams. We also find the quenching and fluorescence rates, i.e., $k_{\rm Q}$ and $k_{\rm fl}$, strongly influence the spatial resolution in a CW STED system. The FWHM of the effective fluorescent spot decreases rapidly with decreasing $k_{\rm Q}$ and $k_{\rm fl}$. This observation is supported by the experimental results of Neupane *et al.*[7]

Therefore, a proper selection (or development) of new fluorescent dyes with smaller k_Q and k_{fl} can be used as an effective method to increase the spatial resolution of a CW STED system. Based on numerical simulations, the theoretical model is determined to be highly consistent with reported experimental results. Despite the smaller power ratio of the STED and excitation beams, CW STED systems utilizing YFP citrine and pTDI dyes show better performance for realizing higher spatial resolutions compared with Atto 565 and 647N dyes.

As a fantastic super-resolution optical method, the STED technique has undergone rapid development. This investigation provides us with an important theoretical basis for the future development of CW STED microscopy. The results serve as a reminder that intrinsic dynamic processes with short lifetimes are still important even in a superficially steady fluorescent system.

In addition, since all of the relevant time constants are of the order of 1 ns or less, one can predict that the statistically steady state of a CW STED can also be realized by utilizing pulsed excitation and depletion lasers with pulse widths of the order of 10 ns. Therefore, we can construct a nanosecond STED system with a high spatial resolution without the need for precise temporal synchronization, as is required in a picosecond STED system, or the occurrence of large thermal effects, as can be found in a CW STED system.

Acknowledgement

The authors appreciate discussion with Bin Yang.

References

[1] Klar T A and Hell S W 1999 *Opt. Lett.* **24** 954
[2] Hell S W and Wichmann J 1994 *Opt. Lett.* **19** 780
[3] Hell S W, Sahl S J, Bates M, Zhuang X, Heintzmann R, Booth M J, Bewersdorf J, Shtengel G, Hess H, Tinnefeld P, Honigmann A, Jakobs S, Testa I, Cognet L, Lounis B, Ewers H, Davis S J, Eggeling C, Klenerman D, Willig K I, Vicidomini G, Castello M, Diaspro A and Cordes T 2015 *J. Phys. D: Appl. Phys.* **48** 443001
[4] Sydor A M, Czymmek K J, Puchner E M and Mennella V 2015 *Trends in Cell Biology* **25** 730
[5] Moneron G, Medda R, Hein B, Giske A, Westphal V and Hell S W 2010 *Opt. Express* **18** 1302
[6] Kuang C, Zhao W and Wang G 2010 *Review of Scientific Instruments* **81** 053709
[7] Neupane B, Chen F, Sun W and Chiu D T 2013 *Review of Scientific Instruments* **84** 043701
[8] Fang Y, Wang Y, Kuang C and Liu X 2014 *Opt. Commun.* **322** 169
[9] Willig K I, Harke B, Medda R and Hell S W 2007 *Nature Methods* **4** 915
[10] Harke B, Keller J, Ullal C K, Westphal V, Sch A and Hell S W 2008 *Opt. Express* **16** 4154
[11] Richards B and Wolf E 1959 *Proceedings of the Royal Society of London* **253** 358
[12] Davidson N and Bokor N 2004 *Opt. Lett.* **29** 1318
[13] Hein B, Willig K I and Hell S W 2008 *Proc. Natl. Acad. Sci. USA* **105** 14271
[14] Hotta J I, Fron E, Dedecker P, Janssen K P, Li C, Müllen K, Harke B, Bückers J, Hell S W and Hofkens J 2010 *J. Am. Chem. Soc.* **132** 5021
[15] Heikal A A, Hess S T, Baird G S, Tsien R Y and Webb W W 2000 *Proc. Natl. Acad. Sci. USA* **97** 11996
[16] Braeken E, Cremer G D, Marsal P, Pèpe G, Müllen K and Vallée R A L 2009 *J. Am. Chem. Soc.* **131** 12201
[17] Luo D, Kuang C, Liu X and Wang G 2013 *Optics & Laser Technology* **45** 723
[18] Lakowicz J R 2006 *Principles of Fluorescence Spectroscopy* (3rd Edn.) (New York: Springer)
[19] Westphal V and Hell S W 2005 *Phys. Rev. Lett.* **94** 143903
[20] Fila M and Hulshof J 1991 *Proceedings of the American Mathematical Society* **112** 473